Metamaterial-Inspired Efficient Electrically Small Antenna

Erentok, Aycan; Ziolkowski, R. W.

Published in:
I E E E Transactions on Antennas and Propagation

Link to article, DOI:
10.1109/TAP.2008.916949

Publication date:
2008

Document Version
Publisher's PDF, also known as Version of record

Metamaterial-Inspired Efficient Electrically Small Antennas

Aycan Erentok, *Member, IEEE*, and Richard W. Ziolkowski, *Fellow, IEEE*

***Abstract*—Planar two-dimensional (2D) and volumetric three-dimensional (3D) metamaterial-inspired efficient electrically-small antennas that are easy to design; are easy and inexpensive to build; and are easy to test; are reported, i.e., the EZ antenna systems. The proposed 2D and 3D electrical- and magnetic-based EZ antennas are shown to be naturally matched to a 50 Ω source, i.e., without the introduction of a matching network. It is demonstrated numerically that these EZ antennas have high radiation efficiencies with very good impedance matching between the source and the antenna and, hence, that they have high overall efficiencies. The reported 2D and 3D EZ antenna designs are linearly scalable to a wide range of frequencies and yet maintain their easy-to-build characteristics. Several versions of the 2D EZ antennas were fabricated and tested. The measurement results confirm the performance predictions. The EZ antennas systems may provide attractive alternatives to existing electrically-small antennas.**

***Index Terms*—Antenna efficiency, antennas, electrically small antenna (ESA), metamaterials.**

I. Introduction

SINCE THEIR potential impact is large, there always has been an interest in electrically-small antenna (ESA) technologies [1]–[9]. We immediately remind the reader of several quantities of interest in describing any antenna using the IEEE standard definitions of terms for antennas, including an ESA [10]. The accepted power (AP) is the power delivered to the antenna terminals from the source. It contains information about any mismatch between the source, the feedline, and the antenna. Let $P_{\rm input}$ be the input power of the source. Let Z_0 be the characteristic impedance of both the source and the feedline, i.e., assume that the feedline is matched to the source. Let $Z_{\rm input}$ be the input impedance of the antenna. The reflection coefficient at the antenna is $\Gamma = (Z_{\rm input} - Z_0)/(Z_{\rm input} + Z_0)$ and the accepted power by the antenna is then $\mathrm{AP} = (1 - |\Gamma|^2)\, P_{\rm input}$, where the mismatch or accepted power efficiency $\mathrm{AE} = \mathrm{AP}/P_{\rm input} = 1 - |\Gamma|^2$. The radiation efficiency is the ratio of the total power radiated to the accepted power, i.e., $\mathrm{RE} = P_{\rm rad}/\mathrm{AP}$. It describes the amount of power that propagates into the far field from the power delivered to the terminals of the antenna, e.g., it is equal to the power accepted by the antenna minus the power dissipated in the antenna. We also introduce another term that takes into account all of the possible losses in a given antenna system, i.e., the overall efficiency. The overall efficiency of the antenna system is then the ratio of the total power radiated to the input power, i.e., $\mathrm{OE} = P_{\rm rad}/P_{\rm input}$. For a 1 W source, it describes what portion of that watt is radiated into the far field of the antenna system. If the directivity of an antenna system is D, its realized gain is $G_R = \mathrm{OE} \times D$. If a is the radius of the smallest sphere enclosing the entire antenna system and if the free space wave number is $k = 2\pi/\lambda_0$, the free space wavelength for a source frequency f_0 being $\lambda_0 = c/f_0$ where c is the speed of light in free space, then the antenna system is said to be electrically small if $ka \leq 1$, i.e., if the antenna is contained within the Wheeler radiansphere. If the antenna system is designed in the presence of an infinite perfect electric conductor (PEC) ground plane, only half the radiansphere is involved and the antenna system is generally said to be electrically small if $ka \leq 0.5$. Even if the PEC ground plane is finite, as will be the case in all of the cases considered below, we will use the latter, more stringent criterion to describe an ESA rather than the former.

Recent technological advances in wireless communications and sensor networks have changed the expectations of antenna designs and their performance. Antennas that are electrically small; are efficient; have significant bandwidth; are inexpensive and easy to build; and integrate simply into more complex systems would fill the needs of many new generation wireless systems if antenna engineers could achieve these goals. Unfortunately, these requirements are contradictory when traditional ESA designs are considered. For instance, without a matching network an ESA is known to have a low overall efficiency because it has an input reactance and resistance that is very poorly matched to a given 50 Ω source. The design of reactance and resistive matching networks is a challenging task that often introduces additional constraints on the overall performance of the resulting system. One common matching network approach is to use a design that would introduce the appropriate conjugate reactance to achieve a total input reactance of zero and then to introduce a quarter-wavelength transformer to match the low input resistance to the source resistance. Thus, the total system, the radiating element *and* the matching circuit, is not electrically small. It is depicted diagrammatically in Fig. 1(a). The concept of the efficient electrically-small antenna (EESA) that we propose below is represented by Fig. 1(b). The entire antenna system: the matching element and the modified radiating element, is contained within the radiansphere. Numerous other

Manuscript received March 6, 2007; revised October 17, 2007.

A. Erentok was with the Department of Electrical and Computer Engineering, University of Arizona, Tucson, AZ 85721–0104 USA. He is now with the Technical University of Denmark, DK-2800 Lyngby, Denmark (e-mail: aer@mek.dtu.dk).

R. W. Ziolkowski is with the Department of Electrical and Computer Engineering, College of Engineering and College of Optical Sciences, University of Arizona, Tucson, AZ 85721–0104 USA (e-mail: ziolkowski@ece.arizona.edu).

Color versions of one or more of the figures in this paper are available online at http://ieeexplore.ieee.org.

Digital Object Identifier 10.1109/TAP.2008.916949

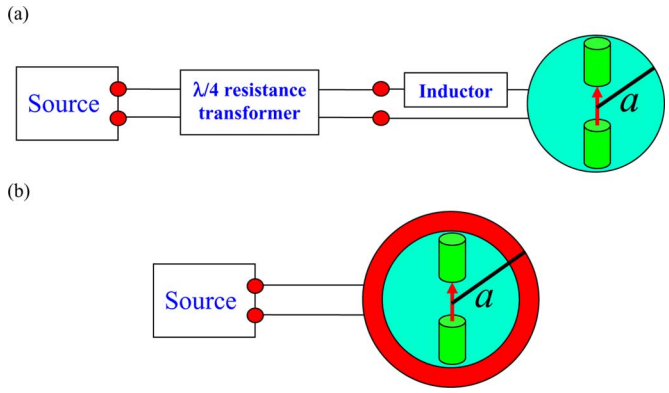

Fig. 1. (a) Traditional electrically small electric dipole antenna system having an inductive element to produce a total input reactance equal to zero, i.e., $X_{\rm ind} = X^*_{\rm ant}$ so that $X_{\rm input} = 0$ and a quarter-wavelength resistance transformer to match the input resistance to the source, and (b) the metamaterial-based EESA paradigm, i.e., the entire antenna system, including the radiating and matching elements, are electrically small defined by the smallest enclosing radiansphere.

matching network approaches have also been considered for ESAs (see, for instance [9, Ch. 9]). Because they rely on various combinations of (circuit and radiating) components, they all have benefits and drawbacks. We are proposing a different paradigm. We will introduce an electrically small parasitic object, essentially one unit cell of the appropriate type of metamaterial, into the extreme near field of the radiator and tailor its characteristics to best utilize the available electrically small design volume to achieve complete matching of the input impedance of the resulting antenna system.

The introduction of the so-called metamaterials (MTMs), artificial materials which have engineered electromagnetic responses that are not readily available in nature, and their exotic properties have provided an alternate design approach that has led to improved performance characteristics of several radiating and scattering systems [11]–[13]. The initial analytical research into the metamaterial-based EESA systems given in [14], [15] revealed that it is possible to design an EESA system formed by an electrically-small electric dipole antenna radiating in the presence of either an idealized homogeneous and isotropic double-negative (DNG) or epsilon-negative (ENG) spherical shell. It was demonstrated that such antenna systems can be made resonant with a radiation efficiency close to unity for ideal lossless metamaterial spherical shells. For instance, the inductive nature of the ENG spherical shell was used to compensate for the capacitive nature of the electrically small dipole antenna to form this resonant radiating system.

These initial studies led to the introduction in [16]–[18] of a metamaterial-based paradigm to achieve an EESA. By "metamaterial-based" we mean that the performance of a bare electric (magnetic) dipole radiating element is modified by surrounding it with an ENG or DNG (mu-negative (MNG) or DNG) metamaterial spherical shell, the spherical shell being an idealized homogeneous, isotropic, lossy, dispersive material. In contrast to the infinitesimal dipole-driven canonical problems in [14], [15] where the radiating element is excited with a constant current, an input impedance can be calculated for the radiating elements in these metamaterial-based EESAs, e.g., a center-fed dipole or coax-fed monopole assigned with finite conductivity and driven using a voltage or current source surrounded by an ENG spherical or hemi-spherical shell. Consequently, the accepted power and overall efficiency of these metamaterial-based EESAs can be calculated for the lossy metamaterial spherical shell driven by the antenna with a finite conductivity. The metamaterial spherical shell can be designed to create a matched resonant antenna system, i.e., the total input reactance is zero and the total input resistance is equal to the resistance of the source. Even when the entire metamaterial-based system, i.e., the metamaterial-shell enclosed radiator, is electrically small, the overall efficiency has been predicted to be 100% when the materials are hypothetically lossless. While theoretically interesting because of their hypothetical performance properties, the metamaterial spherical shells required for these metamaterial-based antenna systems are themselves electrically small, and they have not been realized physically as yet. Nonetheless, progress towards possible realizations of these spherical shells has been made. For example, recently in [19] a slab of DNG metamaterial constructed from a low loss unit cell whose largest dimension is $\lambda_0/75$ has been reported at 400 MHz.

Our theoretical and numerical studies of the radiation and resonance behaviors of these metamaterial-based EESA systems, as well as our efforts to conceptualize structures which might be used to build them, have led to the discovery of several realizable two-dimensional (2D) and three-dimensional (3D) metamaterial-inspired EESA systems. By metamaterial-inspired we mean that the resistive and reactance matching is achieved not with a metamaterial (spherical shell) medium but rather with an element such as an inclusion that has or could be used in a metamaterial unit cell design to realize an ENG, MNG, or DNG medium. In fact, if one of the elements introduced below is placed in a slab unit cell scattering geometry and a material property extraction code is applied to the resulting S-parameters, the metamaterial-inspired element will exhibit the ENG, MNG, or DNG properties required for the corresponding metamaterial-based antenna system, i.e., an ENG (MNG) metamaterial element must be used with an electric (magnetic) dipole radiator. These metamaterial-inspired 2D planar and 3D volumetric EESA systems are easy to design; are easy and inexpensive to build; are easy to test; and, hence, are called EZ antenna systems. The design and performance characteristics of both 2D and 3D electrical- and magnetic-based EZ antennas are reported. They are shown to be naturally matched to a 50 Ω source and shown to have high overall efficiencies. It is demonstrated that these 2D and 3D EZ antenna systems are linearly scalable to a wide range of frequencies without any significant fabrication limitations. Several versions of the 2D EZ antennas were fabricated and tested. It also will be shown that the measured accepted and radiated power results agree rather favorably with their predicted values.

Section II introduces several 3D and 2D magnetic-based EZ antenna designs that are implemented with MNG metamaterial-inspired structures, i.e., respectively, an extruded 3D capacitively-loaded loop (CLL) element, and planar interdigitated and lumped-element CLL elements, driven by an electrically-small circular or rectangular semi-loop antenna which is coaxially-fed through a finite PEC ground plane. The design details and radi-

ation characteristics of each antenna system at several different frequencies are reported. The 3D and 2D electric-based EZ antenna systems dual to those given in Section II are considered in Section III. They are implemented with ENG metamaterial-inspired structures, i.e., respectively, a 3D helical cylindrical strip and a 2D meander line, that are excited by a electrically-small monopole antenna which is coaxially-fed through a finite PEC ground plane. Similarly, the design details and radiation characteristics of each electric-based metamaterial-inspired EZ antenna at several different frequencies are presented. Several of the 2D magnetic- and electric-based metamaterial-inspired EZ antennas were fabricated and tested. It will be demonstrated in Section IV that the measured S_{11} reflection coefficients and the measured total radiated power compare very favorably with the simulated data. A summary of the research findings established in this paper is then given in Section V. An Appendix provides the explicit details of the ANSOFT HFSS (High Frequency Structure Simulator) models that were used to predict the performances of the EZ antenna systems.

II. Magnetic-Based EZ Antenna Systems

A. Three-Dimensional Realizations

The MTM-inspired element is a 3D extrusion of the planar CLL element that was used previously as the unit cell inclusion to realize the volumetric artificial magnetic conductor (AMC) introduced in [20] which was then used as the enabling technology for the low-profile antenna demonstrated in [21]. The design specifications of the proposed 3D magnetic-based EZ antenna with its metamaterial-inspired matching/radiating element are illustrated in Fig. 2. This design was first introduced in [22].

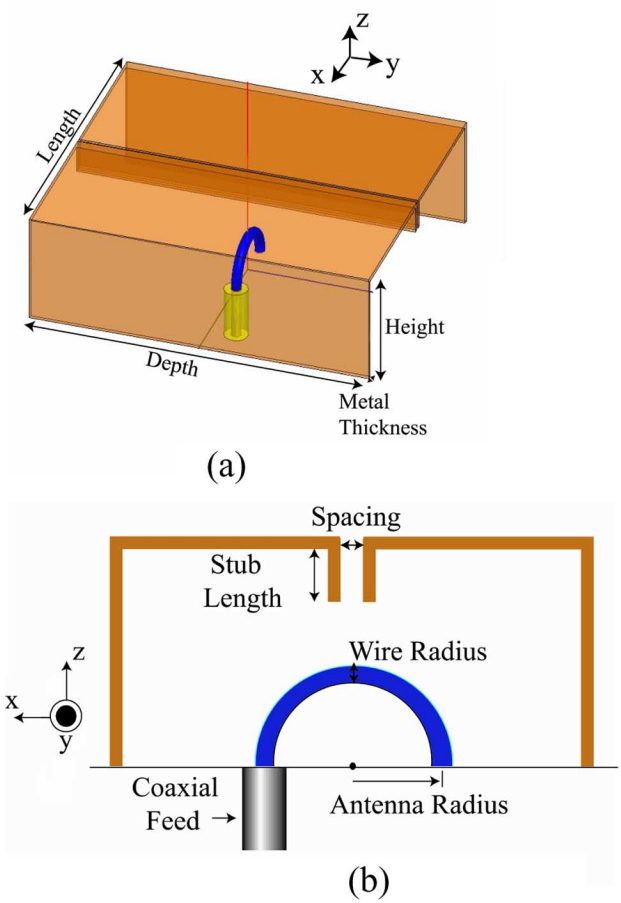

Fig. 2. The 3D magnetic-based EZ antenna geometry and the detailed specifications of each design variable. (a) 3D view and (b) 2D cross-sectional view.

The extruded capacitive element provides a large capacitance which allows the resulting CLL to have a finer tuning capability. Moreover, the extended surface provides an effective region that efficiently captures and resonantly magnifies the magnetic flux generated by the electrically-small semi-circular loop antenna that is driving it. The changes in time of this resonantly-large magnetic flux create the induced currents on the extruded CLL structure and produce correspondingly large electric fields between two stub arms. These strong electric fields create a capacitance in the system that is sufficiently large to match both the inductance due to the current path formed by the extruded CLL structure and the ground plane, and the inductance of the electrically-small semi-circular loop antenna. Thus, the extruded electrically-small CLL structure is a self-resonant reactive element that can be further matched to the reactance part of the electrically-small semi-loop circular antenna to create a resonant RLC tank circuit. The bend radius (taking the wire to be electrically-thin) of the semi-circular loop plays a major role in our ability to tailor the resistance of the radiating element to match it to the feedline resistance, thus achieving a resonant behavior of the overall antenna system. In particular, increasing the radius of the semi-circular loop enhances the resonant coupling of the driving antenna to the radiating extruded CLL element and, thus, enhances the resulting radiation resistance of the antenna system. The length and height (stub depth, length and spacing) of the metamaterial-inspired element provides the major inductance (capacitance) of this antenna design. The thickness of the wire loop and the metal thickness contribute some to the inductance, but their overall effect on the system is very limited. They do, however, significantly impact the conductor losses of the overall antenna system.

Tables I and II give the variable specifications of four different 3D magnetic-based EZ antenna designs at three different frequencies: 300, 1580, and 6000 MHz. Table III summarizes the HFSS predicted radiation characteristics of these antenna systems. The half-power matched *VSWR* fractional bandwidth, discussed in [7], was used to compute the Q value for each system at the resonance frequency $f_0 = \omega_0/2\pi$: i.e., $Q_{\mathrm{VSWR}}(\omega_0) = 2/\mathrm{FBW}_{\mathrm{VSWR}}(\omega_0)$. The ratio, Q_{ratio}, of this Q_{VSWR} value and the Chu limit value $Q_{\mathrm{Chu}} = 1/ka+1/(ka)^3$ was obtained using

$$Q_{\mathrm{ratio}}(\omega_0) = 2/[\mathrm{FBW}_{\mathrm{VSWR}}(\omega_0)Q_{\mathrm{Chu}}(\omega_0) \times \mathrm{RE}]. \quad (1)$$

We note that the presence of losses broadens the resonance and, hence, increases the bandwidth. The inclusion of the radiation efficiency factor, *RE*, in the calculation of the quality factor compensates for this broadening. The copper metal used in Design 1 was assumed to have a 5.8×10^{17} *Siemens/m* conductivity, i.e., to model the copper essentially as a perfect electric conductor

TABLE I
3D MAGNETIC-BASED EZ ANTENNA RESONANT FREQUENCY SPECIFICATIONS, WIRE LOOP DETAILS, AND GROUND PLANE DIMENSIONS

	Design Frequency (MHz)	Loop Antenna Radius (*mm*)	Metal Wire Radius (*mm*)	Ground Plane (x × y) (mm^2)
Design 1*	300	1.9	0.3	520 x 520
Design 2	300	2.8	0.3	520 x 520
Design 3	1580	3.1	0.3	135 x 135
Design 4	6000	0.8	0.07	30.34 x 30.34

* The copper conductivity value for Design 1 was assumed to be 5.8×10^{17} *Siemens/m*. For Designs 2-4 the copper conductivity value was 5.8×10^{7} *Siemens/m*.

TABLE II
3D MAGNETIC-BASED EZ ANTENNA METAMATERIAL INSPIRED STRUCTURE DIMENSIONS AT 300, 1580, AND 6000 MHZ

	Height along *z*-axis (*mm*)	Length along *y*-axis (*mm*)	Depth along *x*-axis (*mm*)	Spacing along *y*-axis (*mm*)	Stub Length along *z*-axis (*mm*)	Copper Metal Thickness (*mm*)
Design 1	10	20	20	0.03	5.741	0.254
Design 2	10	20	20	0.03	5.76	0.254
Design 3	6.5	17.3	20	0.2	1.57	0.254
Design 4	1.625	4.34	5	0.05	0.459	0.0762

TABLE III
SUMMARY OF THE 3D MAGNETIC-BASED EZ ANTENNA RADIATION CHARACTERISTICS AT 300, 1580, AND 6000 MHZ

	$F_{resonant}$ (MHz)	ka	FBW_{VSWR} (%)	Q_{ratio}	AP (*W*)	RE (%)	OE (%)	D
Design 1	299.69	0.11	0.040	6.68	1	100	100	2.68
Design 2	299.97	0.11	0.197	7.10	0.9969	18.73	18.67	2.68
Design 3	1580	0.49	2.013	9.41	0.9998	96.97	96.95	3.70
Design 4	5997	0.46	2.086	8.48	0.9939	92.67	92.10	3.16

in order to explore the performance of the 3D magnetic-based EZ antenna under these ideal conditions. The conductivity of copper in all of the non-ideal cases was always set equal to its well-known value: 5.8×10^7 *Siemens/m*.

The 300 MHz lossless metal Design 1 produced perfect radiation and overall efficiencies with $\mathrm{ka} = 0.11$, i.e., for $a \approx \lambda_0/57$ the radiation efficiency $\mathrm{RE} = 100\%$ and the accepted power was $\mathrm{AP} = 1.0W$. Since the input power $P_{\mathrm{input}} = 1.0W$ in all cases, the accepted power efficiency was $AE = 100\%$ so that the overall efficiency was $\mathrm{OE} = \mathrm{RE} \times \mathrm{AE} = 100\%$. Thus, this metamaterial-inspired 3D magnetic-based EZ antenna system achieved the theoretical upper bound of the metamaterial-based EESAs discussed above and reported in [16]–[18]. With realistic copper losses, however, the radiation efficiency of Design 2 decreased to $\mathrm{RE} = 18.73\%$. The electric fields associated with this highly resonant structure are large and, consequently, produce large conduction losses. By studying several other scaled 300 MHz versions, one finds that the radiation efficiency for an impedance-matched 3D magnetic-based EZ antenna decreases from the high 90's to zero as the *ka* value decreases from the electrically-small antenna limit to zero. The differences between Designs 1 and 2 demonstrate that the copper losses significantly impact the radiation efficiencies of these resonant systems.

A comparison of the Q values of each antenna design reveals that the amount of energy stored in the designed element, which provides the necessary capacitance, depends on the *ka* value of the system. As the *ka* value approaches zero, the reactance of the loop antenna also approaches zero. This loop antenna behavior leads to less stored energy being required to provide the requisite matching capacitance [9]. On the other hand, as the *ka* value approaches the 0.5 limit, the reactance of the loop antenna becomes more inductive and the antenna system needs to store more energy to achieve matching. The fractional bandwidth results indicate that these resonant designs have very narrow bandwidths. While this may not be an issue for the GPS-frequency Design 3, it may be for a communications band design such as Design 2.

A comparison of Designs 3 and 4 clearly shows that the design frequency and component dimension ratios are almost identical. The 3D magnetic-based EZ antenna can be linearly scaled to any desired frequency. This scaled design was achieved at 300 MHz as well. However, we have elected to re-

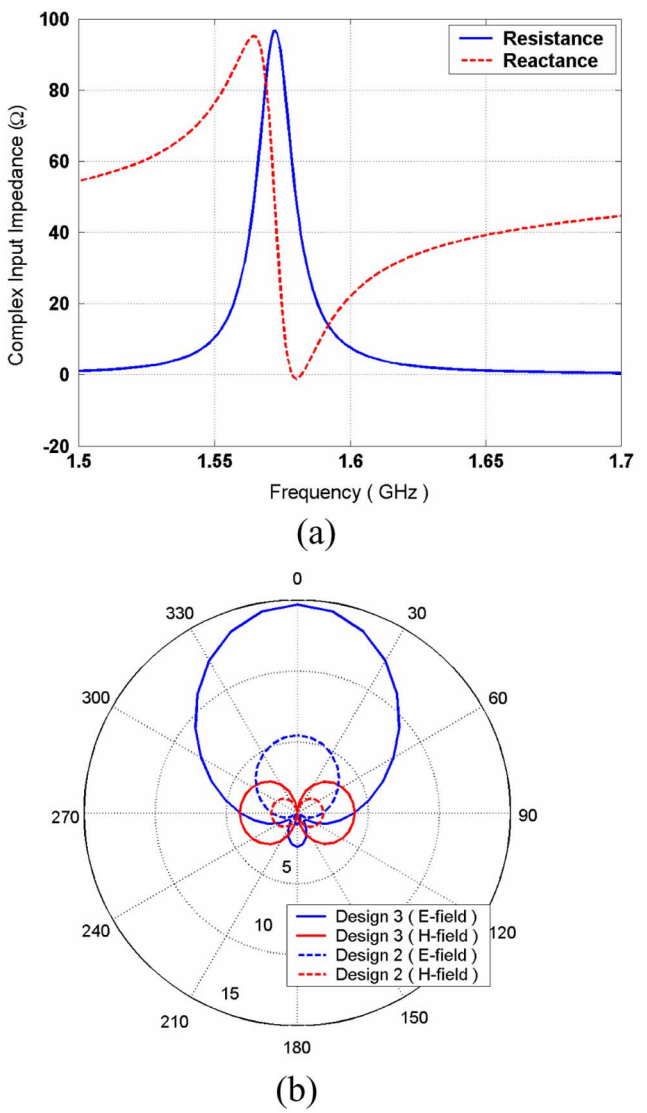

Fig. 3. (a) Complex input impedance values for Design 3 and (b) far-field E- and H-field patterns comparisons for Design 2 and Design 3.

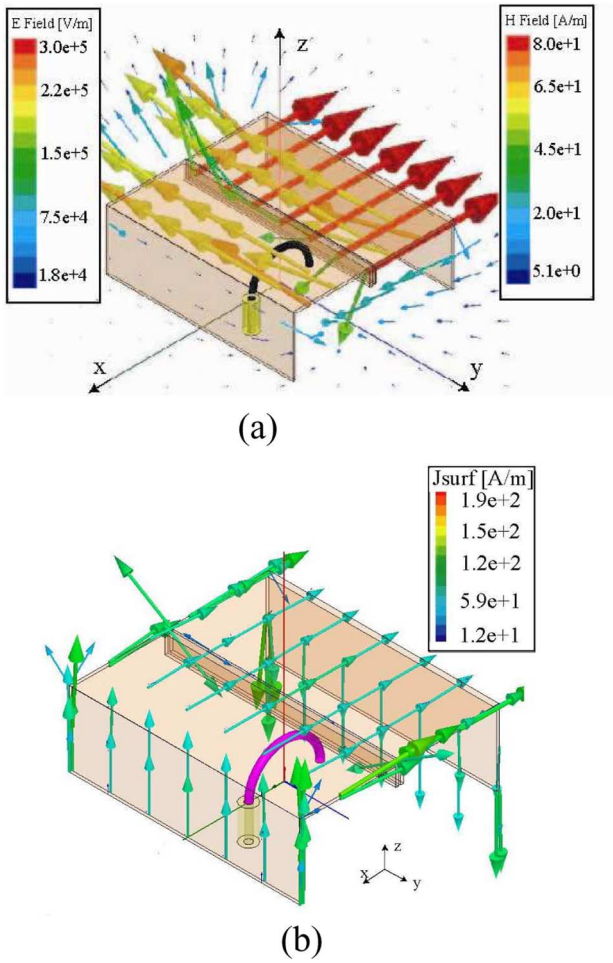

Fig. 4. (a) E- and H-field vector plots, and (b) magnitude of the surface current vectors on the metamaterial-inspired structure obtained from Design 3 at 1580 MHz.

port only the smaller *ka* design at this frequency to allow a direct connection between these results and those reported in [16]. The performance of the scaled limit case $(\mathrm{ka} \sim 0.5)$ at 300 MHz is essentially the same as its higher frequency versions, i.e., the overall efficiencies of these electrically-small-limit antenna systems are very high.

The complex input impedance behavior for the GPS-frequency Design 3 and the far-field radiation pattern comparisons for Designs 2 and 3 are shown in Fig. 3. The resistance and reactance curves in Fig. 3(a) exhibit characteristics analogous to the anti-resonant behavior of an electrically-small circular loop (i.e., a magnetic dipole) antenna [9]. In particular, it is clear from Fig. 3(a) that the 3D magnetic-based EZ antenna is anti-resonant and matched to the feedline at the source frequency. Fig. 3(b) also demonstrates that the 3D magnetic-based EZ antenna is acting like a magnetic dipole over a PEC ground plane. Fig. 4 shows the E- and H-field vector plots using *xy*-plane cuts in the stub region and just above the semi-circular loop antenna, respectively, and the current vector plots on the metamaterial-inspired structure. From Figs. 4(a) and (b), one clearly sees that the metamaterial-inspired radiating structure at resonance provides a uniformly distributed surface current on the extruded CLL element that is induced by the magnetic-fields.

B. Two-Dimensional Realizations

It was elected to try to design planar versions of the EZ antennas to further simplify their fabrication. The 2D magnetic-based EZ antennas designed in this section used Rogers 5880 Duroid$^{\mathrm{TM}}$ with a 31 mils (0.787 mm) thick substrate and a 0.5 oz. (17 μm thick) electrodeposited copper. However, using a dielectric substrate introduces dielectric losses, which further decreases the overall efficiency of the antenna system. Moreover, low-loss dielectric substrates would increase the cost of the design. Nonetheless, the dielectric-backed conductor led to a straightforward fabrication with the facilities available to us. A planar magnetic-based EZ antenna based on a metal-only structure would produce the optimum 2D design.

1) Two-Dimensional Realizations Based on Planar Interdigitated Capacitors: In this section the proposed 3D magnetic-based EZ antenna system is reduced to a planar antenna design first reported in [23]. The 2D planar version of the

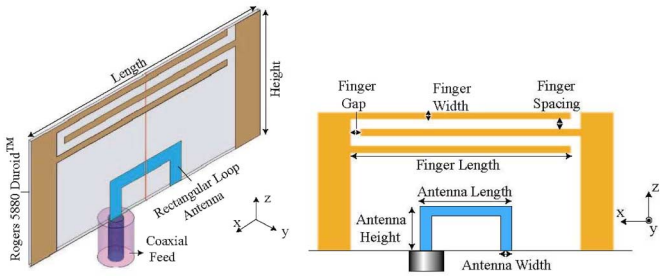

Fig. 5. Geometry and detailed specifications of each design variable for the 2D magnetic-based EZ antenna that incorporates an interdigitated capacitor.

magnetic-based EZ antenna removes the third dimension of the original design, by using instead, a planar interdigitated capacitor for the CLL element. The design specifications of the proposed 2D magnetic-based EZ antenna achieved with its planar metamaterial-inspired matching/radiating element are illustrated in Fig. 5. The capacitor finger number, finger length, gap and spacing between the fingers provide a tuning capability of the resonant frequency. The long and closely spaced capacitor fingers can be used to obtain lower resonant frequencies. The region between the bottom interdigitated capacitor finger and the ground plane captures the magnetic flux generated by the electrically-small rectangular semi-loop antenna that is driving it. The changes in time of this resonantly-large magnetic flux create induced currents on the CLL element which produce a capacitance across the interdigitated finger spacings and gaps. The capacitance obtained from the induced currents is sufficiently large to match both the inductance due to the current path formed by the interdigitated CLL element and the copper ground plane, and the inductance of the electrically-small rectangular semi-loop antenna. The length, width and height of the rectangular semi-loop antenna plays a major role in our ability to tailor the resistance and reactance of the radiating element to the 50 Ω coax-feedline, thus achieving an efficient and electrically-small antenna system. In particular, a larger rectangular semi-loop antenna enhances the resonant coupling of the driving antenna to the 2D interdigitated CLL element and, thus, enhances the resulting radiation resistance and reactance response of the antenna system. The length and height (finger number, finger length, finger spacing and finger gap) of the interdigitated CLL element provides the major inductance (capacitance) of this 2D magnetic-based EZ antenna system. The width of the rectangular semi-loop antenna contributes some to the inductance, but its overall effect to the tuning of the system is limited. The width of the rectangular semi-loop, however, impacts the conductor losses in the antenna system. Independent calculations of the CLL element alone as a unit cell inclusion show that it acts like a MNG medium; this behavior agrees with the predictions in [16], [18] that an MNG metamaterial is required to provide the necessary capacitance to achieve a resonant system and to enable the impedance matching of the inductive rectangular semi-loop antenna to the source.

Tables IV and V give the variable specifications of four different 2D magnetic-based EZ antennas that are achieved with interdigitated capacitor designs at three different frequencies:

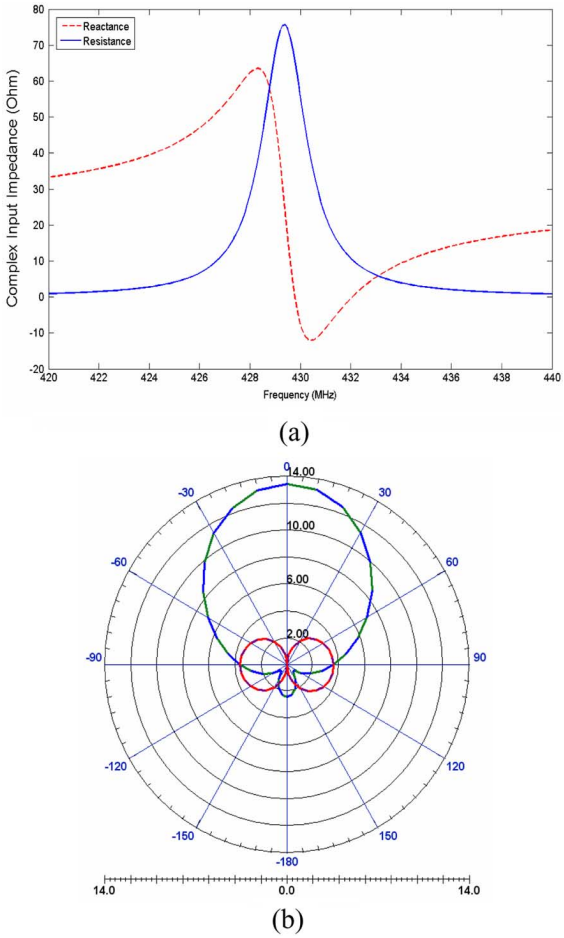

Fig. 6. (a) Complex input impedance values, and (b) far-field E-field (blue) and H-field (red) patterns for Design 6.

300 MHz, 430 MHz and 1580 MHz. Table VI summarizes the HFSS predicted radiation characteristics of these 2D antenna systems. Design 5 was simulated using the idealized lossless copper, $\sigma = 5.8 \times 10^{17}$ *Siemens/m*, and a lossless dielectric substrate to mimic an ideal lossless structure. At 300 MHz it produced an overall efficiency of 99.7%, agreeing with the theoretical predictions presented in the previous section for the 3D magnetic-based EZ antenna. The overall radiation efficiencies decreases from nearly 90% at the electrically-small antenna limit $\mathrm{ka} = 0.5$ to zero as the electrical size of the antenna system decreases. As discussed below in Section IV, Design 6 was fabricated and measured. The predicted complex impedance values and the far-field patterns are shown, respectively in Fig. 6(a) and (b). The anti-resonant nature of the input impedance is apparent; the E-field pattern is clearly a maximum along the normal to the ground plane. Note that because they are electrically small, the patterns in Fig. 6(b) for the 2D magnetic-based EZ antenna are nearly identical to the patterns shown in Fig. 3(b) for the corresponding 3D EZ antenna. Comparisons of the reflection coefficients obtained from the numerical and experimental results demonstrate very good agreement.

The dimensions of the 2D magnetic-based EZ antenna achieved with an interdigitated capacitor are linearly scalable to any desired frequency agreeing with our previous findings. Moreover, the straight forward fabrication process offers an

TABLE IV
2D MAGNETIC-BASED EZ ANTENNA RESONANT FREQUENCY SPECIFICATIONS, RECTANGULAR SEMI-LOOP ANTENNA DETAILS, NUMBER OF INTERDIGITATED CAPACITOR FINGERS AND GROUND PLANE DIMENSIONS

	Design Frequency (MHz)	Antenna Length along *x*-axis (*mm*)	Antenna Height along *z*-axis (*mm*)	Antenna Width (*mm*)	Number of Interdigitated Capacitor Fingers	Ground Plane (x × y) (mm^2)
Design 5*	300	2	1.4	0.6	10	536 × 536
Design 6	430	18	5.2	2.4	10	521 × 521
Design 7	430	25	12	4	3	510 × 510
Design 8	1580	5	3	1	3	137 × 137

* The copper conductivity value for Design 5 was assumed to be 5.8×10^{17} Siemens/m. For Designs 6-8 the copper conductivity value was 5.8×10^{7} Siemens/m.

TABLE V
DIMENSIONS OF THE 2D MAGNETIC-BASED EZ ANTENNA INTEGRATED WITH AN INTERDIGITATED CAPACITOR AT 300, 430, AND 1580 MHZ

	Height along *z*-axis (*mm*)	Length along *y*-axis (*mm*)	Finger Length along *x*-axis (*mm*)	Finger Width along *z*-axis (*mm*)	Finger Gap along *z*-axis (*mm*)	Finger Spacing along *z*-axis (*mm*)
Design 5	9.6	18	10.1	0.254	0.02	0.02
Design 6	38	73	29.8	2.032	1.2192	1.2192
Design 7	38	80	59.7	1.9	2.7	2.7
Design 8	10	22	10.5	0.7	0.15	0.15

attractive alternative to existing designs, e.g., a 60 GHz version has been designed and its measurement results will be reported elsewhere. This property can be seen from the frequency and component dimension ratios of Designs 7 and 8. The radiation efficiency comparisons of Designs 6 and 7 also show that the copper losses significantly impact the overall efficiency of the 2D magnetic-based EZ antenna achieved with an interdigitated capacitor. This occurs because the antenna system is highly resonant. Consequently, it is observed that an important practical criterion is to design the antenna system using a minimum number of interdigitated capacitor fingers to reduce the copper losses and, thus, to enhance the overall efficiency.

The overall efficiencies of these electrically-small-limit antenna systems are high and slightly less than the 3D magnetic-based EZ antenna predictions. Comparisons of the 2D and 3D magnetic-based EZ antenna systems reveal that for the same design frequency, the 3D magnetic-based EZ antenna design is the more efficient choice between these two designs. The reduction of the extruded CLL element in the 3D magnetic-based EZ antenna design to the planar interdigitated CLL element in the 2D magnetic-based EZ antenna design reduces the amount and magnitude of the current flow on the CLL element and, consequently, reduces the radiation efficiency. The far-field E- and H-field patterns and surface current on the matching/radiating element demonstrates behavior similar to the 3D version, i.e., the 2D magnetic-based EZ antennas also act as horizontal magnetic dipoles over a PEC ground plane. The dielectric loss also contributes an increase of $\sim 2\%$ over the total loss of the 2D magnetic-based EZ antenna achieved with an interdigitated capacitor, where the overall efficiency depends on the frequency of operation.

2) Two-Dimensional Realizations Based on Lumped Element Capacitors: This section discusses another 2D planar magnetic-based EZ antenna design based on replacing the interdigitated capacitor with a lumped element capacitor. The main advantage of such a design is to further reduce the conductor losses and, thus, to increase the overall efficiency of the antenna system. Another advantage associated with using a lumped element capacitor would be the ease in which one could tune the resonant frequency of the antenna system.

The 2D magnetic-based EZ antennas introduced here were achieved with a lumped element capacitor based upon the Mu-Rata high-Q GJM lumped capacitor [24], which was used for the fabricated system discussed in Section IV below. The total length, width and thickness of this capacitor was 1, 0.5, and 0.5 mm, respectively, e.g., the selected capacitor size code (EIA) was 0402.

The design specifications of the proposed 2D magnetic-based EZ antenna achieved with its planar metamaterial-inspired matching/radiating element connected with a capacitor are illustrated in Fig. 7. The region between the bottom matching/radiating element and the finite PEC ground plane captures the magnetic flux generated by the electrically-small rectangular semi-loop antenna that is driving it. The changes in time of this resonantly-large magnetic flux create induced currents on the two "arms" of the matching/radiating element which supplies the necessary current for the capacitor. The capacitance in the antenna system is sufficiently large to match both the inductance due to the current path formed by the matching/radiating element and the copper ground plane, and the inductance of the electrically-small rectangular semi-loop antenna. The length, width and height of the rectangular semi-loop antenna again play major roles in our ability to tailor the resistance and

TABLE VI
SUMMARY OF THE 2D MAGNETIC-BASED EZ ANTENNA INTEGRATED WITH AN INTERDIGITATED CAPACITOR RADIATION CHARACTERISTICS AT 300, 430, AND 1580 MHZ

	$F_{resonant}$ (MHz)	ka	FBW_{VSWR} (%)	Q/Q_{Chu}	AP (W)	RE (%)	OE (%)	D
Design 5	309.557	0.085	0.007	17.21	0.997	100	99.70	2.91
Design 6	430.02	0.475	1.083	20.08	0.992	80.14	79.50	3.78
Design 7	430.42	0.497	1.300	17.26	0.995	87.83	87.40	3.64
Design 8	1577.8	0.492	1.267	19.99	0.997	76.93	76.76	3.66

TABLE VII
LUMPED CAPACITOR-BASED 2D MAGNETIC-BASED EZ ANTENNA RESONANT FREQUENCY SPECIFICATIONS, RECTANGULAR LOOP ANTENNA DETAILS AND GROUND PLANE DIMENSIONS

	Design Frequency (MHz)	Antenna Length along x-axis (mm)	Antenna Height along z-axis (mm)	Antenna Width (mm)	Ground Plane (x × y) (mm^2)
Design 9	100	50	15	6	1640 × 1640
Design 10	450	32	10.4	6	519 × 519
Design 11	1575	8	2	1.5	132 × 132

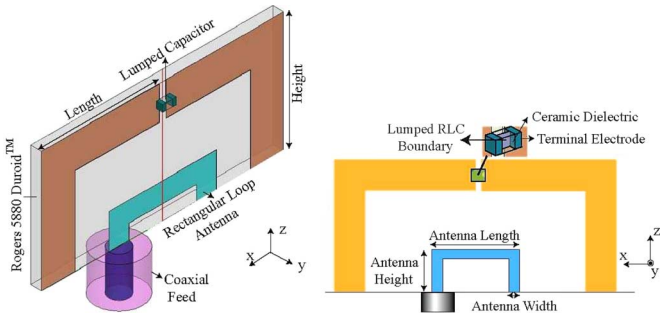

Fig. 7. Geometry and detailed specifications of each design variable for the 2D magnetic-based EZ antenna achieved with a lumped element capacitor.

TABLE VIII
LUMPED CAPACITOR-BASED 2D MAGNETIC-BASED EZ ANTENNA DIMENSIONS AND LUMPED ELEMENT CAPACITANCE VALUES AT 100, 450, AND 1575 MHZ

	Height along z-axis (mm)	Length along y-axis (mm)	Width along y-axis (mm)	Lumped Element Capacitance (pF)
Design 9	70	70	10	15
Design 10	36.8	35.75	10.75	1.5
Design 11	8.3	9.25	3	0.6

reactance of the radiating element to the 50 Ω coax-feedline, thus achieving an EESA system.

The HFSS model of the 2D magnetic-based EZ antenna achieved with a lumped element capacitor uses an estimated replica of the lumped element capacitor. The terminal electrodes and packaging material parameters were assigned as tin and plastic, respectively, to obtain an accurate numerical model of the physical structure. A lumped-RLC boundary condition was applied to a 2D rectangle that stretches between the two terminal electrodes supplying the lumped element capacitance of the antenna system.

Tables VII and VIII give the variable specifications of three different 2D magnetic-based EZ antennas achieved with a lumped element capacitor design at three different frequencies: 100 MHz, 450 MHz and 1575 MHz. The HFSS predicted radiation characteristics of these 2D antenna systems are given in Table IX. As discussed below in Section IV, Design 10 was fabricated and measured. The predicted results were essentially the same as those given in Fig. 6. Comparisons of the reflection coefficients obtained from the numerical and experimental results demonstrate very good agreement. The comparisons of Designs 7 and 10, both of which are close to $ka \sim 0.5$, showed that the 2D magnetic-based EZ antenna achieved with a lumped element capacitor design can further improve the overall efficiency of the antenna system, i.e., the efficiency of Design 10 is approximately 4% larger than Design 7.

III. ELECTRIC-BASED EZ ANTENNA SYSTEMS

This section considers the duals of the 3D and 2D magnetic-based EZ antenna systems that were introduced previously in Section II, i.e., the 3D and 2D electric-based EZ antenna systems are considered below. The first of these 3D and 2D physical realizations of metamaterial-inspired EESAs was obtained by integrating an ENG medium with an electrically-small electric monopole antenna over a finite PEC ground plane. The 3D version uses a 3D cylindrical helix wire strip as a matching element that is excited by an electrically-small monopole. The 2D version is designed as an electrically small printed monopole antenna radiating in the presence of a 2D meander-line. These electric-based EZ antennas are also naturally matched to a 50 Ω source and can be scaled to a wide range of frequencies, e.g., the 2D planar versions again offer an attractive alternative to well-known electric-based electrically-small antenna designs due to their easy-to-build characteristic.

TABLE IX
SUMMARY OF THE LUMPED CAPACITOR-BASED 2D MAGNETIC-BASED EZ RADIATION CHARACTERISTICS AT 100, 450, AND 1575 MHZ

	$F_{resonant}$ (MHz)	ka	FBW_{VSWR} (%)	Q/Q_{Chu}	AP (W)	RE (%)	OE (%)	D
Design 9	98.70	0.202	0.285	14.48	0.996	40.06	39.9	2.79
Design 10	452.52	0.488	1.414	14.28	0.967	92.87	89.8	3.83
Design 11	1576.3	0.417	0.895	17.75	0.999	78.28	78.2	3.58

TABLE X
THE 3D ELECTRIC-BASED EZ ANTENNA RESONANT FREQUENCY SPECIFICATIONS, MONOPOLE ANTENNA AND GROUND PLANE DIMENSIONS

	Design Frequency (MHz)	Monopole Antenna Length along z-axis (mm)	Monopole Antenna Radius (mm)	Ground Plane (x × y) (mm^2)
Design 12	300	11.0	0.5	540 × 540
Design 13	1000	7.4	0.5	182 × 182
Design 14	1300	6.0	0.5	182 × 182

A. Three-Dimensional Realizations

The 3D electric-based EZ antenna uses a 3D cylindrical helical thin copper metal strip that captures the electric field radiated by an electric monopole antenna in its near-field region to produce a large induced current flow on the copper metal strip. The large induced current flow on such an electrically-small multi-turn helical copper metal strip creates an inductance that can be used to form a natural RLC matching element. In particular, the inductance produced by this system is sufficiently large to achieve a match to the large capacitance of the electrically-small monopole antenna.

The design specifications of the proposed 3D electric-based EZ antenna are illustrated in Fig. 8. The 3D cylindrical copper helix is positioned in very close proximity to the monopole antenna, and a tiny copper block is added to the beginning of its first turn to ensure the connectivity between the 3D cylindrical helical strip and the finite ground plane. The number of pitch turns in the electrically-small 3D helical strip can be adjusted to provide the necessary inductance to form the RLC matching element. The electric field distribution induces current along the helix, which then creates a magnetic field and, hence, the desired inductance. Increasing the pitch length, the distance between two turns in the 3D helix structure along its axis, reduces the total inductance in the antenna system due to the lower copper strip density. The monopole antenna height determines the magnitude of the resonant coupling of the driving antenna to the 3D helical strip. Reducing the monopole antenna height weakens the resonant RLC behavior and, thus, the resonance effect diminishes for very short, electrically-small monopole antennas. On the other hand, the length of the monopole antenna plays a major role in our ability to tailor the resistance of this radiator in order to match it to the 50 Ω source and, therefore, to achieve an electric-based EESA system. Increasing the helix width and decreasing the pitch length both provide a larger inductance to the resonant system. The monopole antenna radius itself affects the reactance part of this electric-based antenna system. A smaller antenna radius is necessary to produce a larger inductive value in order to maintain the resonance effect. This behavior agrees with our earlier numerical predictions given in [16]. Because they are electrically thin, the monopole antenna radius and copper metal thickness have an impact on the conductor losses and, thus, the overall efficiency of the 3D electric-based EZ antenna system. The multi-turn helix wire is closely placed to the monopole, and thus the losses resulting from the changes in the current distributions due to the associated proximity effects can be as large as those corresponding to the skin effect alone.

Tables X and XI give the variable specifications of three different 3D electric-based EZ antenna designs at three different frequencies: 300, 1000, and 1300 MHz. The HFSS predicted radiation characteristics of these 3D antenna systems are given in Table XII. The overall radiation efficiencies of the 3D electric-based antenna systems depend on their electrical sizes agreeing with what was determined for the dual, magnetic cases. It decreases from nearly 85% at the electrically-small antenna limit $ka = 0.5$ to zero as the electrical size of the antenna system decreases. The predicted complex input impedance and corresponding S_{11} values for a 50 Ω source obtained from Design 14 are given in Fig. 9. Tables X and XI demonstrate that the antenna system can be designed at any desired frequency mainly by tuning the helix radius and the monopole antenna length. Comparisons of the $\mathrm{FBW_{VSWR}}$ for the 3D electric-based and magnetic-based antenna systems show that the electric-based designs provide larger $\mathrm{FBW_{VSWR}}$ bandwidths, i.e., the magnetic-based antenna systems for the same electrical length have about 50% less $\mathrm{FBW_{VSWR}}$ due to their anti-resonant behavior. The far-field radiation patterns obtained from Design 14 are given in Fig. 10. The far-field E-field pattern, the solid red curve in Fig. 10, does not provide an exact match to the well-known monopole antenna radiation pattern, because the ground plane is finite.

B. Two-Dimensional Realizations

The proposed 3D electric-based EZ antenna was reduced to a planar design by integrating an electrically small printed

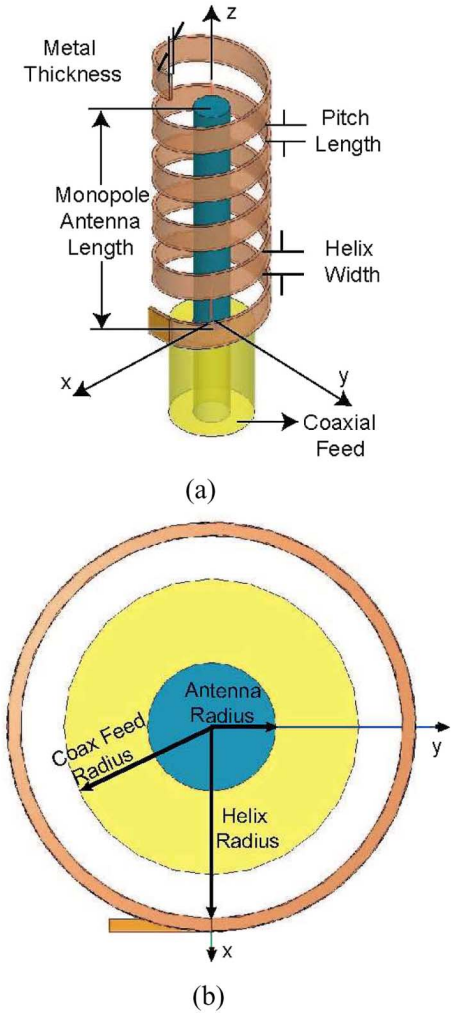

Fig. 8. Geometry and detailed specifications of each design variable for the 3D electric-based EZ antenna (a) 3D view and (b) 2D cross-sectional view.

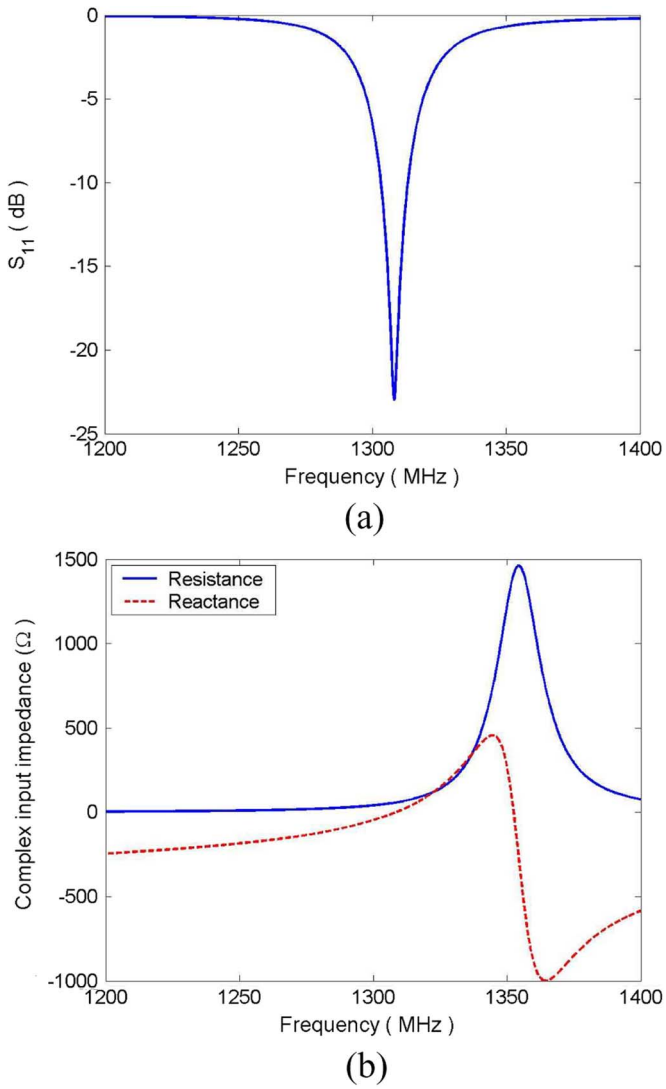

Fig. 9. (a) S_{11} values, and (b) complex input impedance values for the 3D electric-based EZ antenna Design 14.

monopole antenna with a 2D meander-line structure over a finite ground plane. The bottom of the 2D meander-line is connected directly to the finite ground plane. The design specifications of the proposed 2D electric-based EZ antenna achieved with a planar 2D meander-line matching element are illustrated in Fig. 11. Independent calculations of the meander-line element alone as a unit cell inclusion show that it acts like a ENG medium; this behavior agrees with the predictions in [16]–[18] that an ENG metamaterial is required to provide the necessary inductance to achieve a resonant system and to enable the impedance matching of the capacitive monopole antenna to the source.

The extended 2D copper surface of the meander-line serves as a current path for the induced current generated by the electric-field distribution of the electrically-small printed monopole antenna fed through a finite PEC ground plane. The 2D meander-line is positioned in very close proximity to the monopole antenna, approximately $\lambda_0/275$. It provides a large inductance, which again allows the combined system to form an RLC resonator. Another valid explanation for the properties of the inductance can be made if one visualizes each electrically-small copper strip as a transmission line terminated in a short circuit. The complex impedance of such a transmission line is inductive. The entire meander-line can then be thought of as a series of inductors that are driven by the electrically-small printed monopole antenna and, consequently, it provides enough inductance to achieve the desired matching system. Increasing the antenna height enhances the resonant coupling of the driving printed monopole antenna to the 2D meander-line; and thus, it enhances the resulting resonant response of the antenna system. A thinner substrate thickness would also enhance the resonant coupling between the antenna and the 2D meander-line. The antenna width affects the reactance part of this antenna system, where a smaller printed dipole width requires a larger inductive value to maintain the resonance effect. This behavior also agrees with our numerical predictions given earlier in [16]. The mutual capacitance between the copper strips strictly depends on the distance that separates them. Increasing the distance between two copper strips in the meander-line reduces the mutual coupling; and, therefore, the resonance behavior shifts towards lower frequencies. The resonant effect, however, is reduced due

TABLE XI
THE 3D ELECTRIC-BASED EZ ANTENNA METAMATERIAL-INSPIRED STRUCTURE DIMENSIONS AT 300, 1000, AND 1300 MHZ

	Pitch Length along z-axis (mm)	Helix Width along x-axis (mm)	Number of Helix Turns	Copper Helix radius (mm)	Metal Thickness (mm)
Design 12	1.5	0.8	10	5	0.8
Design 13	1.5	0.8	10	1.7	0.8
Design 14	1.6	0.8	10	1.5	0.1

TABLE XII
SUMMARY OF THE 3D ELECTRIC-BASED EZ ANTENNA RADIATION CHARACTERISTICS AT 300, 1000, AND 1300 MHZ

	$F_{resonant}$ (MHz)	ka	FBW_{VSWR} (%)	Q/Q_{Chu}	AP (W)	RE (%)	OE (%)	D
Design 12	306.9	0.1	0.437	4.30	0.968	13.74	13.3	0.95
Design 13	1035.8	0.347	1.575	6.08	0.995	77.48	77.1	1.14
Design 14	1308	0.462	2.379	8.01	0.994	84.95	84.52	1.35

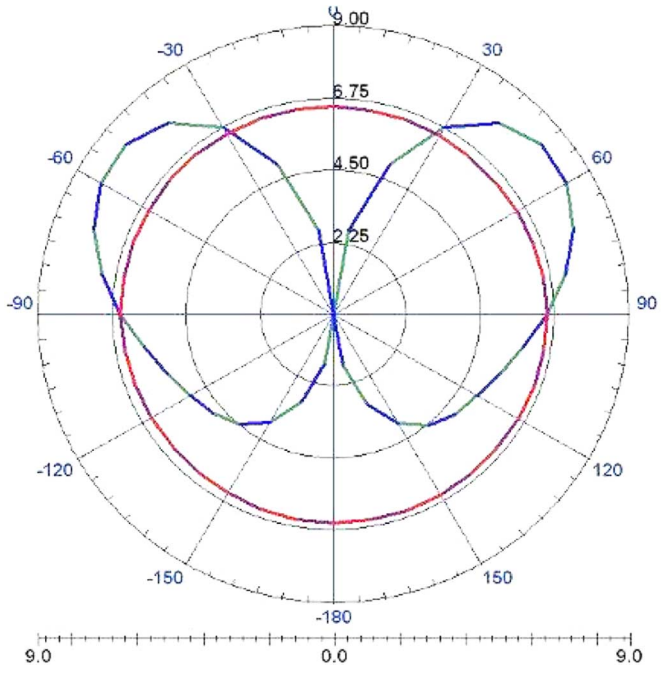

Fig. 10. E-field (blue) and H-field (red) patterns obtained at 1308 MHz for the 3D electric-based EZ antenna Design 14.

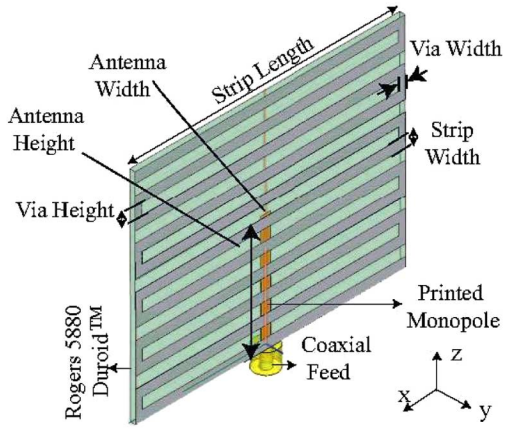

Fig. 11. Geometry and detailed specifications of each design variable for the 2D electric-based EZ antenna.

to the lower copper strip density, i.e., the strip density determines the amount of current induced by the electric field distribution. Increasing the strip length and decreasing the strip width both provide larger inductance to the resonant system, but with different magnitudes. Again, this resonance phenomenon can be explained using transmission line theory. The proposed antenna design is electrically small and, thus, each strip length should be much smaller than $\lambda_0/4$. Consequently, the characteristic impedance of the given transmission line, i.e., the inductive value of the proposed design, should increase as a tangent function when a longer strip length is used providing that the overall length still remains smaller than $\lambda_0/4$. Reducing the strip width, on the other hand, provides a logarithmic increase of the inductance dictated by the strip width and the substrate thickness ratio. The electric-based 2D EZ antennas reported here were designed using Rogers 5880 Duroid$^{\mathrm{TM}}$ with a 31 mils (0.787 mm) thick substrate and a 0.5 oz. (17 μm) electrodeposited copper.

Tables XIII and XIV give the variable specifications of three different 2D electric-based EZ antenna designs at two different frequencies: at 430 and 1373 MHz. The HFSS predicted radiation characteristics of these 2D antenna systems are given in Table XV. The overall radiation efficiencies of the 2D electric-based antenna systems depend on the electrical size of the antenna system agreeing with all of our findings given above. In contrast to Design 16, Design 15 demonstrates a well-balanced smaller, yet reasonably efficient design. As discussed below in Section IV, Design 17 was fabricated and measured. The predicted complex impedance values and the far-field patterns for Design 17 are shown, respectively in Fig. 12(a) and (b). The expected resonant nature of the input impedance is apparent; the E-field pattern is clearly a maximum along ground plane as is expected for this monopole configuration. Note that because

TABLE XIII
3D ELECTRIC-BASED EZ ANTENNA RESONANT FREQUENCY SPECIFICATIONS, PRINTED MONOPOLE ANTENNA AND GROUND PLANE DIMENSIONS

	Design Frequency (MHz)	Monopole Antenna Height along z-axis (*mm*)	Monopole Antenna Width along x-axis (*mm*)	Ground Plane (x × y) (mm^2)
Design 15	430	17.0	1.5	442 × 442
Design 16	430	28.0	1.5	500 × 500
Design 17	1373	8.3	1.5	156 × 156

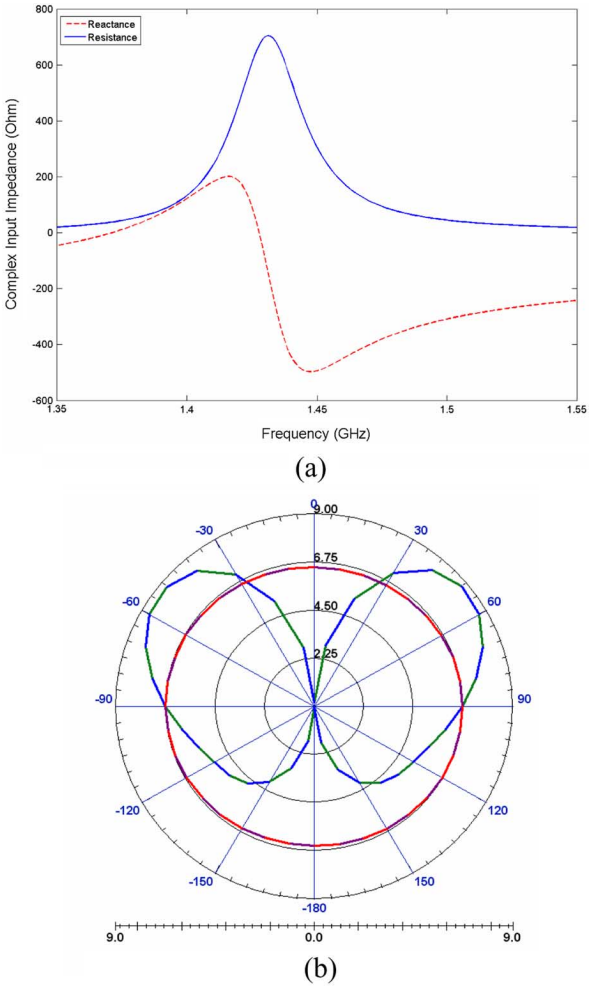

Fig. 12. (a) Complex input impedance values, and (b) far-field E-field (blue) and H-field (red) patterns for Design 17.

they are electrically small, the patterns in Fig. 12(b) for the 2D electric-based EZ antenna are nearly identical to the patterns shown in Fig. 10 for the corresponding 3D EZ antenna.

IV. PROOF-OF-CONCEPT EXPERIMENTS

In order to validate the numerical predictions, several of the 2D magnetic- and electric-based EZ antennas were fabricated and tested. Because of a limitation in available measurement tools and expertise, we could only measure S-parameters in our laboratory. To obtain at least one set of efficiency measurements, we fabricated samples of one design and sent them to the National Institute of Standards and Technology (NIST) in Boulder, CO for testing.

In particular, Design 6 was fabricated using a photolithography technique and was mounted on a 0.8 mm thick copper ground plane. The S-parameters were measured with an HP 8720C network analyzer calibrated with the standard SOLT method. The simulated and measured S_{11} values of the fabricated Design 6 antenna system are compared in Fig. 13. The measured S_{11} values show a very good agreement with the simulated data, where the resonant frequency is only 1.88% different from the measured value of 438.1 MHz. The measured $\mathrm{FBW}_{\mathrm{VSWR}}$ was 1.3%, in very good agreement with the predicted value.

Design 10 was also fabricated using a photolithography technique and was mounted on a 0.8 mm thick copper 15 mm × 15 mm ground plane, and then copper taped to a larger 521 mm × 521 mm copper ground plane. The measured S_{11} values shown in Fig. 14 demonstrate a very good agreement with the HFSS predictions, where the resonant frequency is only 0.7% below the measured value of 455.8 MHz. The measured $\mathrm{FBW}_{\mathrm{VSWR}}$ was 1.5%, in very good agreement with the predicted value.

Two copies of the 2D electric-based EZ antenna, Design 17, were fabricated again using a photolithography technique, and each of them was mounted on a 0.8 mm thick, 156 mm × 156 mm large copper ground plane as shown in Fig. 15. While the total power radiated by an ESA has been measured in a variety of ways, each has its own foibles [26]. It was decided to use the reverberation chamber at NIST-Boulder for the power efficiency measurements of Design 17 at the recommendation of Dr. Chris Holloway [27].

A reverberation chamber is basically a shielded room (grounded high conducting metallic walls) with an arbitrarily shaped metallic paddle that rotates (stirrer or tuner) [28]. The rotating paddle creates a statistically uniform environment throughout the working volume of the chamber [29]. Initially, reverberation chambers were used as high-field-amplitude test facilities for electromagnetic interference (EMI) and compatibility (EMC) effects. Reverberation chambers are currently being used for a wide range of other measurement applications, which include, but are not limited to, determining: 1) radiated immunity of components and large systems; 2) radiated emissions; 3) shielding characterizations of cables, connectors, and materials; 4) antenna efficiency; 5) probe calibration; 6) characterization of material properties; 7) absorption and heating properties of materials; and 8) biological and biomedical

TABLE XIV
2D MATCHING MEANDER-LINE ELEMENT DIMENSIONS AT 430 AND 1373 MHZ

	Total Height (*mm*)	Copper Strip Length (*mm*)	Copper Strip Width (*mm*)	Number of Copper Strips	Via Height (*mm*)	Via Width (*mm*)
Design 15	33.274	41	1.524	11	1.651	1.016
Design 16	46.15	49.5	4.75	5	5.6	3.1
Design 17	14.732	18	1.524	5	1.778	1.016

TABLE XV
SUMMARY OF THE 2D ELECTRIC-BASED EZ ANTENNA RADIATION CHARACTERISTICS AT 430 AND 1373 MHZ

	$F_{resonant}$ (MHz)	ka	FBW_{VSWR} (%)	Q/Q_{Chu}	AP (*W*)	RE (%)	OE (%)	D
Design 15	429.9	0.352	2.32	5.77	0.999	57.86	57.80	1.18
Design 16	430.4	0.494	3.60	5.9	0.996	93.10	92.75	1.46
Design 17	1373	0.497	4.079	5.35	0.985	89.34	88.00	1.44

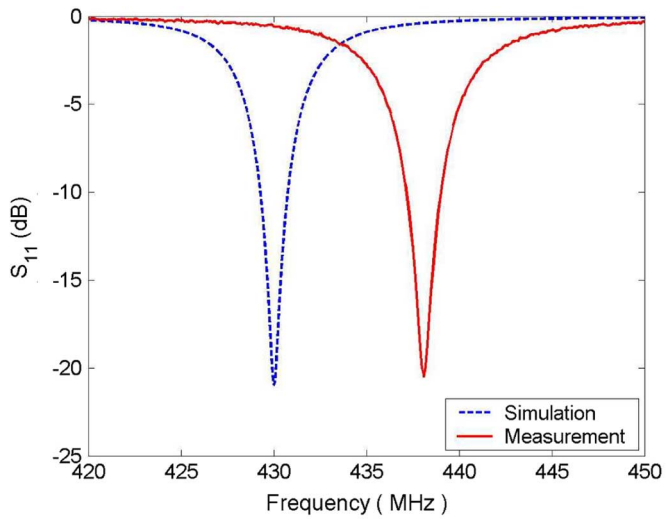

Fig. 13. Predicted and measured S_{11} values for the 2D magnetic-based EZ antenna integrated with an interdigitated capacitor obtained from Design 6 at 430 MHz.

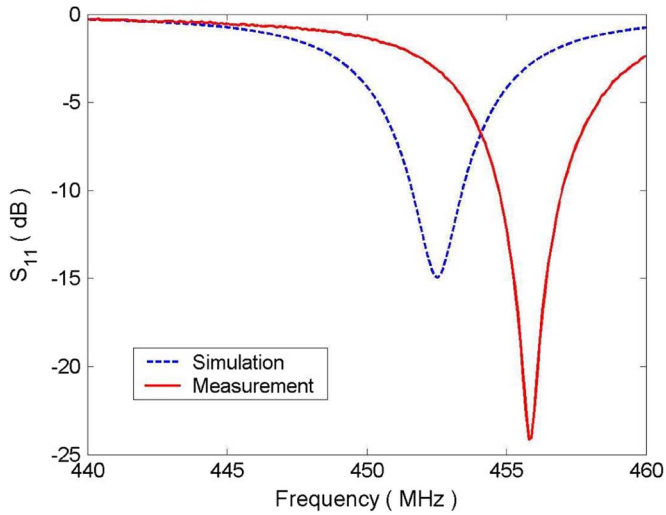

Fig. 14. Design 10 predicted and measured S_{11} values for the 2D magnetic-based EZ antenna achieved with a lumped element capacitor at 450 MHz.

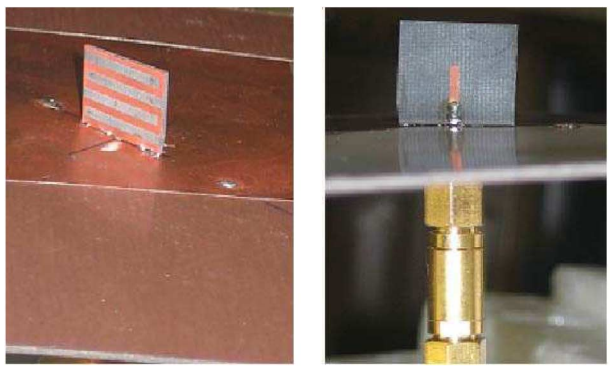

Fig. 15. The fabricated 2D electric-based EZ antenna, Design 17, which was designed to operate at 1373 MHz.

effects. While most of the research and applications of reverberation chambers to date have been geared towards EMC/EMI measurements, applications to antennas and wireless devices began to emerge over the past few years. These include total radiated power and overall efficiency measurements [30], [31]. A summary of the literature for all these types of reverberation chamber measurements can be found in [32].

When a source, i.e., antenna under test (AUT), is placed in a reverberation chamber, the energy radiates from the antenna and interacts with (i.e., reflects off) the chamber walls and paddle. This energy is monitored at a receiving antenna in the chamber. Thus, the total power received at the receiving antenna is the energy balance of the energy radiated by the source minus the energy lost into the chamber walls (and any cables and other objects inside the chamber). Reverberation chambers are an ideal environment for measurements of the total radiated power and overall efficiency of antennas [30], [31]. However, in these types

of measurements the losses in the chamber wall must be calibrated out. This is accomplished by using a known (well characterized) antenna as a *reference* source. In this approach, measurements at the receive antenna are first obtained with the antenna under test. Next, measurements at the receive antenna are taken with the reference source (i.e., the AUT is replaced with the reference antenna). In the NIST reverberation chamber, a dual-ridged horn antenna was used for the reference antenna for all of the measurement results discussed below. The overall efficiency of the horn antenna was determined previously to be 94% [33]. The ratio of the total power received from the AUT to that from the reference antenna gives a measure of the relative total radiated power and, hence, the *relative* overall efficiency (i.e., overall efficiency of the AUT relative to that of the reference antenna). We note that radiated field patterns of the AUT can not be obtained from reverberation chamber measurements.

The predicted and measured S_{11} values, and the measured total radiated power relative to the reference horn antenna for the fabricated 2D electric-based EZ antenna, Design 17, are given in Fig. 16. The measured relative overall efficiency, i.e., the overall efficiency of the Design 17 EZ antenna relative to that of the horn antenna, is approximately equal to or slightly greater than that of the reference horn antenna itself at the design frequency of 1373 MHz. Since the efficiency of the reference horn antenna is 94%, the measured overall efficiency of the Design 17 metamaterial-inspired 2D electric-based EZ antenna system was found to be in excess of 94%. The total radiated power response of the bare monopole antenna relative to the reference horn is also given in Fig. 16(b), e.g., the bare monopole without the metamaterial-inspired near-field parasitic element was obtained by removing the substrate and the associated 2D meander-line. Note that bare monopole antenna is electrically small and it is not resonant at the design frequency. Numerically, it was predicted at 1373 MHz that its input impedance would be $Z_{\text{bare}} = 0.561 - j535.9\Omega$ giving a reflection coefficient magnitude equal to 0.9998 and that its total radiated power would be $P_{\text{rad, bare}} = 3.796 \times 10^{-4} W$. Thus, the ratio of the total power radiated by the bare monopole to the reference horn was predicted to be -33.94 dB. The measured reflection coefficient was $S_{11} = 0.999$ at 1373 MHz, and the measured power ratio was -34.08 dB, both in very good agreement with their predicted values. Consequently, Fig. 16(b) demonstrates, as is well known, that an electrically-small monopole by itself with no matching circuit of any kind is a poor radiator. On the other hand, Fig. 16(b) also demonstrates how the presence of a specifically designed metamaterial-inspired near-field parasitic element can dramatically improve the total power radiated by the bare copper monopole antenna. In particular, it shows that the measured total radiated power of the 2D electric-based EZ antenna at 1373 MHz was approximately 35dB larger than the measured total radiated power of the bare copper monopole antenna, where both individual total radiated power values were obtained relative to the reference horn. These measured results confirm that the design methodologies introduced here and in [16] are valid, and that the theoretical metamaterial-based and physical metamaterial-inspired antenna systems provide an attractive alternative to existing electrically-small antenna designs. The measured FBW_{VSWR} was 4.1%; and, because the radiation efficiency can be obtained from the S_{11} and overall efficiency values at 1376.16 MHz, the corresponding Q and Q/Q_{Chu} values at the resonance frequency were 49.15 and 4.91, respectively, in very good agreement with the predicted value.

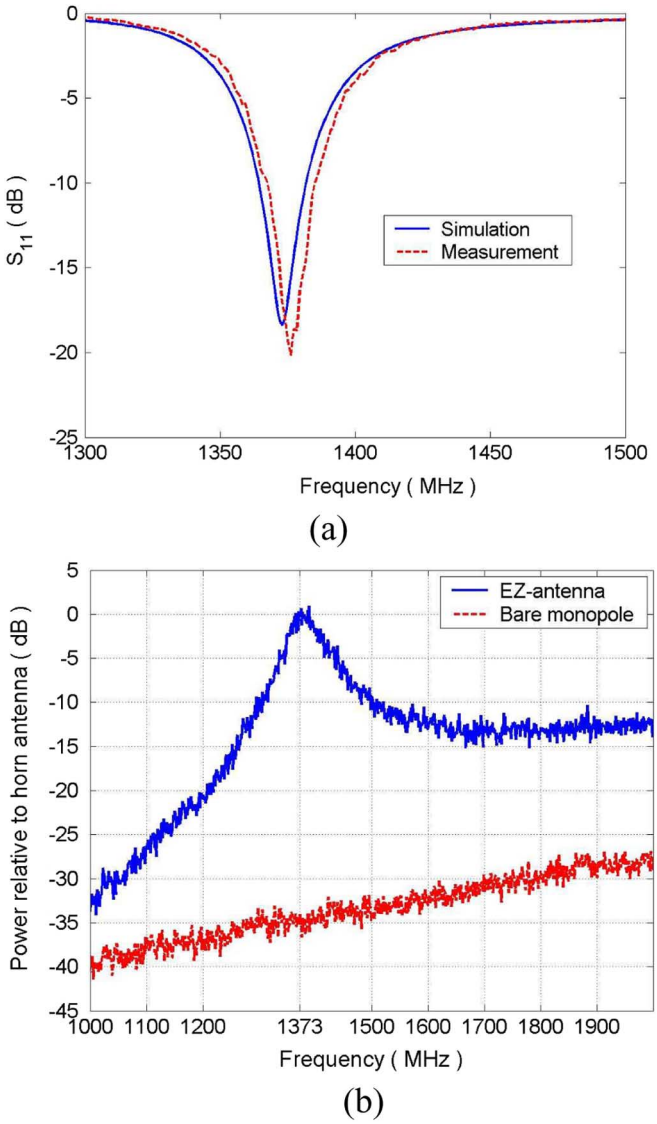

Fig. 16. A comparison of the (a) HFSS predicted and measured S_{11} values obtained for Design 17, and (b) measured total radiated power relative to the reference rectangular horn antenna for Design 17 and for the bare copper monopole antenna.

Fig. 17 demonstrates how the ground plane size affects the S_{11} performance of the 2D electric-based EZ antenna. These measurements were achieved by sacrificing one of the original systems and cutting the ground plane to the indicated sizes. Note that the full ground plane size was determined by the restrictions that are imposed by the HFSS software to obtain accurate far-field antenna radiation values, i.e., the radiation box should be sized at least $\lambda_0/4$ from the source. The measured results, which showed very good accepted power values even for a much smaller ground plane, suggest that it would be possible to further reduce the ground plane size and still obtain a high overall efficiency.

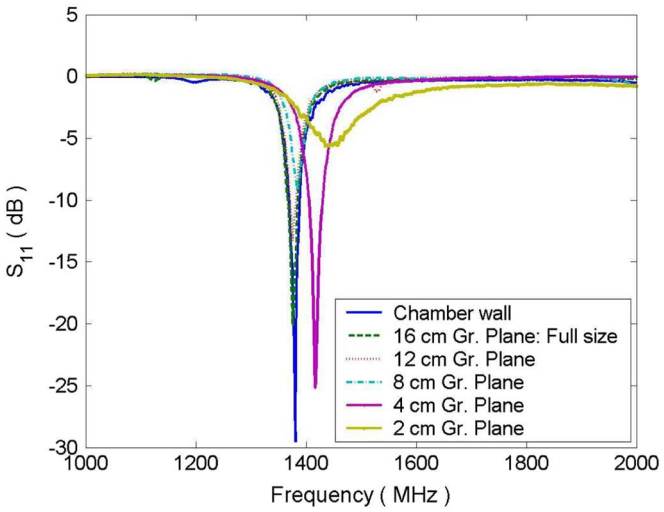

Fig. 17. The effects of the ground plane size on the measured S_{11} values that were obtained for Design 17.

V. Conclusion

The research work presented in this paper focused on the development of metamaterial-inspired EESAs. An EESA design methodology was developed in which a resonant LC structure is achieved by introducing an appropriately designed electrically-small metamaterial-inspired (ENG or MNG) element into the extreme near field of a driven electrically-small (electric or magnetic) antenna.

Magnetic-based EZ antenna systems were realized as inexpensive and easy-to-build EESAs. It was demonstrated that they are linearly scalable to a wide range of frequencies and yet maintain their easy-to-build characteristics. Because of the copper losses in the presence of the resulting resonant field distributions, the overall efficiency of these EESAs depended on the choice of the overall electrical size. Even though complete matching was achieved, the versions whose sizes were far from the electrically-small limit were shown to have large conductor losses because of their resonant nature and, hence, had small overall efficiencies. On the other hand, the electrically-small-limit versions were shown to be highly efficient. The highly electrically-small versions shared this behavior if the copper losses were ignored. In particular, the 3D magnetic-based EZ antenna design details and radiation characteristics at 300, 1580, and 6000 MHz were reported. Alternative planar designs were also proposed by reducing the 3D metamaterial-inspired element to a 2D planar one. In one 2D design, a planar interdigitated CLL element was used; a high-Q lumped element capacitor-based CLL element was used in the other design. The resulting 2D magnetic-based EZ antennas were shown to be an attractive design due to their electrically-small size, high overall efficiency, and yet easy-to-build characteristics. The lumped element design introduced a highly desirable potential tuning capability into the 2D magnetic-based EZ antennas. The 2D magnetic-based EZ antennas were fabricated, and their input reflection coefficients were measured. Comparisons of the reflection coefficients obtained from the numerical and experimental results demonstrate very good agreement.

The 3D and 2D electric-based EZ antennas, which are duals of the 3D and 2D magnetic-based EZ antenna systems, were also considered. The 3D and 2D realizations of these electric-based metamaterial-inspired EESAs were obtained by integrating an effective ENG medium with an electrically small printed monopole antenna fed through a finite ground plane. The 3D version used a 3D cylindrical helical thin copper metal strip as a matching element that is excited by an electrically-small monopole. The 2D version was designed as an electrically small printed monopole antenna radiating in the presence of a 2D meander-line. These 2D and 3D electric-based EZ antennas are also naturally matched to a 50 Ω source, can be scaled to a wide range of frequencies without any compromise in their performance, and are inexpensive and easy-to-build. The design details and radiation characteristics were reported, respectively, at 300, 1000, and 1300 MHz for the 3D electric-based EZ antennas and at 430 and 1373 MHz for the 2D versions. The 3D electric-based EZ antennas were shown to have $\mathrm{FBW}_{\mathrm{VSWR}}$ bandwidths that were larger than their dual magnetic-based EZ antenna designs having the same electrical size. The total far-field radiated power, hence overall efficiency, and the input reflection coefficients of the 1373 MHz version of the 2D electric-based EZ antenna designs were measured in the reverberation chamber facility at NIST Boulder. These experimental results confirmed the numerical predictions of their performance.

The MTM-inspired EESA design methodology introduced in this paper and the initial proof-of-concept EESAs realized with this approach may provide attractive alternatives to existing electrically-small antennas. We recently have scaled electric EZ antennas down to the HF and VHF bands and magnetic EZ antennas up to the millimeter-wave band. In the high frequency bands, for example at 60 GHz, the interdigitated 2D magnetic EZ antenna systems have advantages over existing lumped element based matching networks and ESA designs simply because circuit components associated with existing design methodologies are not readily available there. On the other hand, in the low frequency bands, lumped element versions of the electric and magnetic EZ antennas can take advantage of readily available small size, large value inductors and capacitors, respectively, to achieve highly subwavelength ESA designs. These lower and higher frequency designs will be reported elsewhere in the near future.

Appendix
HFSS Simulation Models For Magnetic-Based EZ Antennas

The HFSS models of the 3D magnetic-based EZ antennas consist of three components: a) a semi-circular loop copper wire antenna connected to the finite PEC ground plane and fed by a 50 Ω coaxial-cable, b) an extruded CLL copper

structure with its two "J-sheets" being connected to the finite PEC ground plane and with a specified vacuum gap being uniformly held between the capacitor legs of these sheets, and c) a vacuum radiation box that surrounds the antenna system. The HFSS model of the 2D magnetic-based EZ antenna consists of three components: a) a rectangular semi-loop copper antenna connected to a finite PEC ground plane and fed by a 50 Ω coaxial-cable, b) a pre-determined number of interdigitated capacitor fingers that are uniformly positioned with the same gap and spacing across each element and with its two main "arms" being connected to the finite PEC ground plane, and c) a vacuum radiation box that surrounds the antenna system. The HFSS model of the lumped capacitor based 2D EZ antenna consists of three components: a) a rectangular semi-loop copper antenna connected to a finite PEC ground plane and fed by a 50 Ω coaxial-cable, b) a lumped element capacitor connected between two main "arms" which are connected to a finite PEC ground plane, and c) a vacuum radiation box that surrounds the antenna system. The distance between the two main "arms" was determined by the physical length of the capacitor. The terminal electrodes and ceramic material parameters were assigned as tin and ceramic, respectively, to obtain an accurate numerical model of the physical structure. A lumped-RLC boundary condition was applied to a 2D rectangle that stretches between the two terminal electrodes supplying the lumped element capacitance of the antenna system. The default HFSS electrical properties were assigned for the copper, i.e., $\varepsilon = \varepsilon_0$, $\mu = \mu_0$, and $\sigma = 5.8 \times 10^7 \mathrm{Siemens/m}$. The radiation box for each design was created using a cube that is at least $\lambda_0/4$ distance away from the capacitive element per ANSOFT instructions and that has one face being assigned as the finite PEC ground plane. This requirement fixes the size of the ground plane. Initial meshing was applied to improve the convergence of each simulation.

Another numerical model for the 2D magnetic-based integrated with a lumped capacitor, an HFSS and ANSOFT Designer hybrid simulation method, was also used to validate the accuracy of the imposed lumped-RLC boundary condition by using the measured capacitor data library provided by Panasonic [24]. In order to use the Panasonic lumped capacitor library, the lumped-RLC boundary condition was replaced with a lumped port in the HFSS design and all the other design variables were kept the same. Next, the HFSS model was inserted into the ANSOFT Designer as a sub-circuit and simulated with the measured Panasonic capacitor values. We preferred to use only the HFSS numerical model since it provided more information about the antenna system radiation characteristics.

ACKNOWLEDGMENT

This work was supported in part by DARPA Contract Number HR0011-05-C-0068. The authors would like to thank Dr. Christopher L. Holloway and Mr. John Ladbury, NIST Boulder, for carrying out the reverberation chamber antenna measurements and for providing useful inputs to the measurement section discussion.

REFERENCES

[1] L. J. Chu, "Physical limitations of omnidirectional antennas," *J. Appl. Phys.*, vol. 19, pp. 1163–1175, Dec. 1948.
[2] H. A. Wheeler, "Fundamental limitations of small antennas," in *IRE Proc.*, Dec. 1947, vol. 35, pp. 1479–1484.
[3] H. A. Wheeler, "The radiansphere around a small antenna," *IRE Proc.*, vol. 47, pp. 1325–1331, Aug. 1959.
[4] R. E. Collin and S. Rothschild, "Evaluation of antenna Q," *IEEE Trans. Antennas Propag.*, vol. AP-12, pp. 23–27, Jan. 1964.
[5] R. C. Hansen, "Fundamental limitations in antennas," *Proc. IEEE*, vol. 69, pp. 170–181, Feb. 1981.
[6] J. S. McLean, "A re-examination of the fundamental limits on the radiation Q of electrically small antennas," *IEEE Trans. Antennas Propag.*, vol. 44, pp. 672–676, May 1996.
[7] A. D. Yaghjian and S. R. Best, "Impedance, bandwidth, and Q of antennas," *IEEE Trans. Antennas Propag.*, vol. 53, pp. 1298–1324, Apr. 2005.
[8] R. P. Harrington, *Time Harmonic Electromagnetic Fields*. New York: McGraw-Hill, 1961, pp. 414–420.
[9] C. A. Balanis, *Antenna Theory*, 3rd ed. New York: Wiley, 2005, pp. 637–641.
[10] "IEEE standard definitions of terms for antennas," 1993, 145–1993,.
[11] N. Engheta and R. W. Ziolkowski, "A positive future for double negative metamaterials," *IEEE Microw. Theory Tech*, vol. 53, pp. 1535–1556, Apr. 2005.
[12] N. Engheta and R. W. Ziolkowski, Eds., *Metamaterials: Physics and Engineering Explorations*. Hoboken, NJ: Wiley-IEEE Press, 2006.
[13] A. Alù, N. Engheta, A. Erentok, and R. W. Ziolkowski, "Single-negative, double-negative and low-index metamaterials and their electromagnetic application," *IEEE Antennas Propag. Mag.*, vol. 49, no. 1, pp. 23–36, Feb. 2007.
[14] R. W. Ziolkowski and A. Kipple, "Application of double negative metamaterials to increase the power radiated by electrically small antennas," *IEEE Trans. Antennas Propag.*, vol. 51, pp. 2626–2640, Oct. 2003.
[15] R. W. Ziolkowski and A. D. Kipple, "Reciprocity between the effects of resonant scattering and enhanced radiated power by electrically emall antennas in the presence of nested metamaterial shells," *Phys. Rev. E.*, vol. 72, Sep. 2005, 036602,.
[16] R. W. Ziolkowski and A. Erentok, "Metamaterial-based efficient electrically small antennas," *IEEE Trans. Antennas Propag.*, vol. 54, pp. 2113–2130, Jul. 2006.
[17] R. W. Ziolkowski and A. Erentok, "At and beyond the chu limit: Passive and active broad bandwidth metamaterial-based efficient electrically small antennas," *IET Microw., Antennas Propag.*, vol. 1, pp. 116–128, Feb. 2007.
[18] A. Erentok and R. W. Ziolkowski, "A hybrid optimization method to analyze metamaterial-based electrically small antennas," *IEEE Trans. Antennas Propag.*, vol. 55, pp. 731–741, Mar. 2007.
[19] A. Erentok, R. W. Ziolkowski, J. A. Nielsen, R. B. Greegor, C. G. Parazzoli, M. H. Tanielian, S. A. Cummer, B.-I. Popa, T. Hand, D. C. Vier, and S. Schultz, "Low frequency lumped element-based negative index metamaterial," *Appl. Phys. Lett.*, vol. 91, p. 184104, Nov. 2007.
[20] A. Erentok, P. Luljak, and R. W. Ziolkowski, "Antenna performance near a volumetric metamaterial realization of an artificial magnetic conductor," *IEEE Trans. Antennas Propag.*, vol. 53, pp. 160–172, Jan. 2005.
[21] A. Erentok, D. Lee, and R. W. Ziolkowski, "Numerical analysis of a printed dipole antenna integrated with a 3D AMC block," *IEEE Antennas Wireless Propag. Lett.*, vol. 6, pp. 134–136, 2007.
[22] A. Erentok and R. W. Ziolkowski, "An efficient metamaterial-inspired electrically-small antenna," *Microw. Opt. Tech. Lett*, vol. 49, no. 6, pp. 1287–1290, 2007.
[23] A. Erentok and R. W. Ziolkowski, "Two-dimensional efficient metamaterial-inspired electrically-small antenna," *Microw. Opt. Tech. Lett*, vol. 49, no. 7, pp. 1669–1673, 2007.
[24] [Online]. Available: http://www.murata.com/cap/index.html(11/29/2006)
[25] [Online]. Available: http://industrial.panasonic.com(11/29/2006)
[26] D. Pozar and B. Kaufman, "Comparison of three methods for the measurement of printed antenna efficiency," *IEEE Trans. Antennas Propag.*, vol. 36, pp. 136–139, Jan. 1988.
[27] C. Holloway, "Private communications," 2007.
[28] *Electromagnetic Compatibility (EMC): Part 4: Testing and Measurement Techniques. Section. 21: Reverberation Chambers. International Electrotechnical Commission (IEC)*, IEC 61000-4-21.

[29] D. A. Hill, "Electromagnetic theory of reverberation chambers," *NIST Technical Note 1506,* National Institute of Standards and Technology. Boulder, CO, 1998.
[30] N. Serafimov, P.-S. Kildal, and T. Bolin, "Comparison between radiation efficiencies of phone antennas and radiated power of mobile phones measured in anechoic chambers and reverberation chambers," in *Proc. IEEE Antennas and Propagation Int. Symp.*, Jun. 2002, vol. 2, pp. 478–481.
[31] K. Rosengren, P.-S. Kildal, C. Carlsson, and J. Carlsson, "Characterization of antennas for mobile and wireless terminals in reverberation chambers: Improved accuracy by platform stirring," *Microw. Opt. Technol. Lett.*, vol. 30, no. 20, pp. 391–397, Sep. 2001.
[32] C. L. Holloway, D. A. Hill, J. M. Ladbury, P. Wilson, G. Koepke, and J. Coder, "On the use of reverberation chambers to simulate a controllable Rician radio environment for the testing of wireless devices," *IEEE Trans. Antennas Propag., Special Issue on Wireless Communications*, vol. 54, no. 11, pp. 3167–3177, Nov. 2006.
[33] J. Ladbury, G. Koepke, and D. Camell, "Evaluation of NASA Langley Research Center mode-stirred chamber facility," *NIST Tech. Note 1508*, p. 106, Jan. 1999.

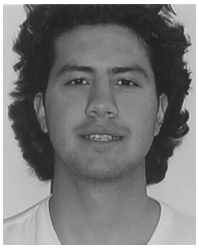

Aycan Erentok (M'07) received the B.S. (*cum laude* and honors), M.S., and Ph.D. degrees in electrical engineering from the University of Arizona, Tuscon, in 2001, 2003 and 2007, respectively.

He is currently employed as a Postdoctoral Research Fellow at the Technical University of Denmark, Lyngby. His current research interests include EM optimization algorithms, electrically small antennas and effects of metamaterials on antenna performance. He also spent summer 2006 at the ATD/DPD (INTEL Chandler Campus) and worked on system level power delivery network measurements using IFDIM methodology.

Richard W. Ziolkowski (M'97–SM'91–F'94) received the Sc.B. degree in physics (*magna cum laude* with honors) from Brown University, Providence, RI, in 1974 and the M.S. and Ph.D. degrees in physics from the University of Illinois at Urbana-Champaign, in 1975 and 1980, respectively.

He was a member of the Engineering Research Division, Lawrence Livermore National Laboratory, CA, from 1981 to 1990 and served as the Leader of the Computational Electronics and Electromagnetics Thrust Area for the Engineering Directorate from 1984 to 1990. He joined the Department of Electrical and Computer Engineering, University of Arizona, Tuscon, as an Associate Professor in 1990, was promoted to Full Professor in 1996, and was selected by the Faculty to serve as the Kenneth Von Behren Chaired Professor, for 2003 to 2005. He currently is serving as the Litton Industries John M. Leonis Distinguished Professor. He holds a joint appointment with the College of Optical Sciences at the University of Arizona. His research interests include the application of new mathematical and numerical methods to linear and nonlinear problems dealing with the interaction of acoustic and electromagnetic waves with complex media, metamaterials, and realistic structures.

Prof. Ziolkowski is a member of Tau Beta Pi, Sigma Xi, Phi Kappa Phi, the American Physical Society, the Optical Society of America, the Acoustical Society of America, and Commissions B (Fields and Waves) and D (Electronics and Photonics) of the International Union of Radio Science (URSI). He was awarded the Tau Beta Pi Professor of the Year Award in 1993 and the IEEE and Eta Kappa Nu Outstanding Teaching Award in 1993 and 1998. He served as the Vice Chairman of the 1989 IEEE/AP-S and URSI Symposium in San Jose, and as the Technical Program Chairperson for the 1998 IEEE Conference on Electromagnetic Field Computation. He was an Associate Editor for the IEEE TRANSACTIONS ON ANTENNAS AND PROPAGATION from 1993 to 1998. He served as a member of the IEEE Antennas and Propagation Society (AP-S) Administrative Committee (ADCOM) from 2000 to 2002. He served as the IEEE AP-S Vice President in 2004 and President in 2005. He is currently serving as a Past-President member of the AP-S ADCOM. He was a Steering Committee Member for the 2004 ESA Antenna Technology Workshop on Innovative Periodic Antennas. He served as a co-Chair of the International Advisory Committee for the inaugural IEEE International Workshop on Antenna Technology: Small Antennas and Novel Metamaterials, IWAT2005, and as a member of the International Advisory Committee for IWAT 2006 and 2007. He was a member of the International Advisory Committee for the IEEE 2005 International Symposium on Microwave, Antenna, Propagation and EMC Technologies, MAPE2005. He served as an Overseas Corresponding Member of the ISAP2007 Organizing Committee. He was a Co-Guest Editor for the October 2003 IEEE TRANSACTIONS ON ANTENNAS AND PROPAGATION Special Issue on Metamaterials. For the US URSI Society he served as Secretary for Commission B (Fields and Waves) from 1993 to 1996 and as Chairperson of the Technical Activities Committee from 1997 to 1999, and as Secretary for Commission D (Electronics and Photonics) from 2001 to 2002. He served as a Member-at-Large of the U.S. National Committee (USNC) of URSI from 2000 to 2002 and is now serving as a member of the International Commission B Technical Activities Board. He is a Fellow of the Optical Society of America. He was a Co-Guest Editor of the 1998 special issue of the *Journal of the Optical Society of America A* featuring Mathematics and Modeling in Modem Optics. He was a Co-Organizer of the Photonics Nanostructures Special Symposia at the 1998, 1999, 2000 OSA Integrated Photonics Research (IPR) Topical Meetings. He served as the Chair of the IPR sub-committee IV, Nanostructure Photonics, in 2001.